General tooth boundary conditions for equation free modelling

A. J. Roberts[*]   I. G. Kevrekidis[†]

June 12, 2006

arXiv:math.DS/0603433 v1   17 Mar 2006

Abstract

We are developing a framework for multiscale computation which enables models at a "microscopic" level of description, for example Lattice Boltzmann, Monte Carlo or Molecular Dynamics simulators, to perform modelling tasks at "macroscopic" length scales of interest. The plan is to use the microscopic rules restricted to small "patches" of the domain, the "teeth", using interpolation to bridge the "gaps". Here we explore general boundary conditions coupling the widely separated "teeth" of the microscopic simulation that achieve high order accuracy over the macroscale. We present the simplest case when the microscopic simulator is the quintessential example of a partial differential equation. We argue that classic high-order interpolation of the macroscopic field provides the correct forcing in whatever boundary condition is required by the microsimulator. Such interpolation leads to Tooth Boundary Conditions which achieve arbitrarily high-order consistency. The high-order consistency is demonstrated on a class of linear partial differential equations in two ways: firstly through the eigenvalues of the scheme for selected numerical problems; and secondly using the dynamical systems approach of holistic discretisation on a general class of linear PDEs. Analytic modelling shows that, for a wide class of microscopic systems, the subgrid fields and the effective macroscopic model are largely independent of the tooth size and the particular tooth boundary conditions. When applied to patches of

[*]Computational Engineering and Sciences Research Centre, Department of Maths & Computing, University of Southern Queensland, Toowoomba, Queensland 4352, Australia. mailto:aroberts@usq.edu.au

[†]Program in Applied and Computational Mathematics, Princeton University, Princeton, NJ 08544, USA. mailto:yannis@Princeton.edu

microscopic simulations these tooth boundary conditions promise efficient macroscale simulation. We expect the same approach will also accurately couple patch simulations in higher spatial dimensions.

Keywords: multiscale computation, gap tooth scheme, coupling boundary conditions, high order consistency

Contents

1 Introduction

The components of physical systems often operate on vastly different space and time scales (Dolbow, Khaleel & Mitchell 2004). We must somehow simulate such systems on the scale of interest and operation. But systems that depend on physical processes at multiple scales pose notorious difficulties. These multiscale difficulties are major obstacles to progress in fields as diverse as environmental and geosciences, climate, materials, combustion, high energy density physics, fusion, bioscience, chemistry, power grids and information networks (Dolbow et al. 2004).

Here we further develop the equation free approach to multiscale modelling (Kevrekidis et al. 2003). Given a numerical simulator for physical components at much smaller scales than the scale of primary interest, the aim of the methodology is to bridge the space and time scales to simulations resolving the macroscale of interest. Here we focus on bridging *space scales*

by improving the accuracy of the gap-tooth methodology for microsimulators (Gear et al. 2003, Samaey et al. 2004, 2005). Crucially, our gap-tooth methods must adapt to whatever microsimulator code is provided; one key application of this work is to microsimulators that are tried and tested legacy codes that we do not want to modify.

The equation-free approach provides *on the fly* closure methods which constitute critical components of, for example, mathematical homogenization (Samaey et al. 2005, Gustafsson & Mossino 2003, Balakotaiah & Chang 2003, e.g.), renormalization group techniques (Ei et al. 2000, Mudavanhu & O'Malley 2003, Chorin & Stinis 2005, e.g.), and multiscale finite elements (Hou & Wu 1997, Chen & Hou 2002, e.g.). These closure methods not only need to be computationally efficient but also need to be capable of reproducing the physical dynamics with high fidelity. That is, we seek a methodology that can be systematically refined.

Using microscopic simulators of the one dimensional Burgers' equation, Roberts & Kevrekidis (2005) demonstrated the possibility of achieving high order accuracy in the gap-tooth scheme for macroscale dynamics. The particular microsimulator we use is a fine scale discretization of the PDE which we execute only in the interior of the teeth (see Figure 1). At each time step during execution, the microsimulator within each tooth requires boundary values which must be continuously updated. If the microsimulator was to be executed over the entire macrodomain, these boundary values would naturally come from the immediately neighboring fine grid; this grid is missing in gap-tooth simulation. That pilot study only considered microsimulators which had boundary conditions of specified *flux* at the edges of their simulation teeth. Here we generalise the analysis to consider microsimulators with either

- Dirichlet boundary conditions of specified field u at the tooth edges, Section 2,

- mixed boundary conditions of specified $av_j \pm b\partial_x v_j$ at the tooth edges, Section 3, or

- nonlocal two-point boundary conditions such as those arising in a microscale discretisation of a PDE, Section 4.

Consider the gap-tooth scheme (Gear et al. 2003, Samaey et al. 2004, e.g.) illustrated in Figure 1. Let $v_j(x, t)$ be the fine scale, microscopic field in the jth tooth, and U_j the jth coarse grid value; that is, the value at the center of each tooth. Let the tooth width be h. Then the edge of a tooth lies at a distance $h/2$ from its coarse grid point, a fraction $r = h/(2H)$ to
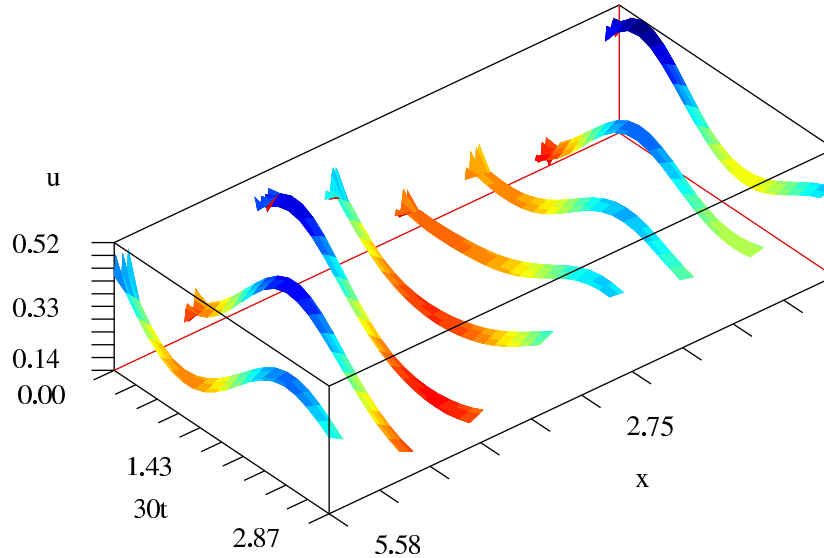
Figure 1: simulation of Burgers' equation using Dirichlet boundary conditions on the teeth (specified u on the edges).

the next coarse grid point. The amount of computation performed by microsimulators is proportional to the width of the (microscale) teeth. Hence we aim for the fraction r to be as small as possible, so that the teeth are a relatively small part of the physical domain and the computational cost minimised. The coupling rule developed in Sections 2, 3 and 4 is that you *obtain whatever values are necessary for the boundaries of the microscopic simulators by classic interpolation of the* macroscopic *grid values from neighbouring teeth.* As a nonlinear example of the coupling we develop, Figure 1 shows a gap-tooth simulation of the nonlinear dynamics of Burgers' equation in one spatial dimension.

This coupling rule promotes a strong connection between classic finite difference discretisations of PDEs, classic finite elements, and the methodology of the gap-tooth scheme. First, the PDE acts as the quintessential example of a microsimulator in that it informs us of the dynamics in an 'infinitesimal patch'. The only difference between the gap-tooth scheme and the spatial discretisation of PDEs is that the microsimulators in the gap-tooth scheme encode the dynamics on *small finite patches*, whereas the PDE encodes the dynamics on *infinitesimal* patches. Consequently, classic interpolation serves the same role in both: namely, the interpolation appropriately transfers information from the macroscale of interest to the microscale simulators. Second, the theoretical support for the gap-tooth scheme is based upon a subgrid scale structure, as is the classic finite element method. Also, the solvability condi-

tion in the construction of the theoretical gap-tooth model is similar to the Galerkin projection of finite elements. But whereas finite elements *impose* a class of subgrid fields, both the theoretical approach here and the gap-tooth scheme use actual subgrid scale dynamics, obtained from the microsimulator or the PDE, to *obtain* appropriate subgrid scale fields. Thus this approach systematically implements model closures for macroscale discretisations.

In Section 5 we prove that classic interpolation connects accurately the teeth across the gaps for the general *linear* fourth order PDE. The technique of holistic discretisation (Roberts 2001*b*, e.g.) resolves subgrid scale structures to reproduce with high fidelity the dynamics of specified PDEs (Roberts 2002). The techniques were adapted by Roberts & Kevrekidis (2005) to the gap-tooth scheme in the case where the microsimulator requires Neumann boundary conditions of specified slope/flux (see Section 3). Using the same techniques, Section 5 analyses the use of classic interpolation of macroscale grid values in the microscale simulators and shows the following desirable properties:

- the approach generates macroscopic discretisations which are consistent with the microscopic dynamics to high order in the macroscopic tooth separation H;

- the macroscopic model and the microscopic solution field are essentially independent of the size of the teeth, measured by r; and

- the macroscopic model and the microscopic solution field are essentially independent of the details of the tooth boundary conditions (TBCs) that couple the teeth together.

Thus our proposed rule generates gap-tooth schemes that may be systematically refined to high order accuracy, and gives rise to macroscale simulations that are largely independent of irrelevant microscale parameters.

2   Dirichlet teeth (specified ʊ)

In this section we consider the case of microsimulators that require at each time step the field values on the edge of each spatial patch to be specified. We model this case by PDEs with Dirichlet conditions coupling the dynamics in the teeth. The values for these Dirichlet conditions are obtained by interpolation across the gaps between the teeth using finite difference operators and the exact relationships between the operators. When applied to simple diffusion, the resulting scheme has high order accuracy.

Discrete operators are essential in the analysis. Define the shift operator $Eu(x) = u(x + H)$ and equivalently $EU_j = U_{j+1}$ as appropriate for steps on the coarse grid size H. Then we use the following identities for discrete operators (National Physical Laboratory 1961, p.65, e.g.):

$$\text{mean} \quad \mu = \tfrac{1}{2}(E^{1/2} + E^{-1/2})\,, \tag{1}$$

$$\text{difference} \quad \delta = E^{1/2} - E^{-1/2}\,, \tag{2}$$

$$\text{shift} \quad E = 1 + \mu\delta + \tfrac{1}{2}\delta^2\,, \tag{3}$$

$$\text{derivative} \quad H\partial_x = 2\sinh^{-1}\tfrac{1}{2}\delta = \delta - \tfrac{1}{6}\delta^3 + \mathcal{O}(\delta^5)\,, \tag{4}$$

$$\mu^2 = 1 + \tfrac{1}{4}\delta^2\,. \tag{5}$$

Formulae involving these operators become more accurate as the differences δ become small. Such small differences arise either as the macroscopic grid size $H \to 0$ or equivalently as the gradients of the physical field u become small.

For example, Roberts & Kevrekidis (2005) showed arbitrary order consistent macroscopic dynamics from a gap-tooth scheme as the grid size $H \to 0$. The key to that analysis is the following transformation of the operator for evaluating spatial derivatives $H\partial_x$ at the patch boundaries $E^{\pm r}$:

$$E^{\pm r}H\partial_x = (1 + \mu\delta + \tfrac{1}{2}\delta^2)^{\pm r} 2\sinh^{-1}\tfrac{1}{2}\delta\,.$$

But this right-hand side, when expanded in a Taylor series in small differences δ, is composed of terms which have an odd number of centred operators δ and μ. Consequently the right-hand side above would require field values halfway between the grid values. These are unknown. Instead, from (5), multiply the right-hand side by the identity $\mu/\sqrt{1 + \delta^2/4}$, and then expand in small differences δ:

$$\begin{aligned}
E^{\pm r}H\partial_x &= (1 + \mu\delta + \tfrac{1}{2}\delta^2)^{\pm r} 2\sinh^{-1}\tfrac{1}{2}\delta \\
&= \frac{\mu}{\sqrt{1 + \tfrac{1}{4}\delta^2}}(1 + \mu\delta + \tfrac{1}{2}\delta^2)^{\pm r} 2\sinh^{-1}\tfrac{1}{2}\delta \\
&= \mu\delta \pm r\delta^2 - (\tfrac{1}{6} - \tfrac{1}{2}r^2)\mu\delta^3 \mp r(\tfrac{1}{12} - \tfrac{1}{6}r^2)\delta^4 \\
&\quad + (\tfrac{1}{30} - \tfrac{1}{8}r^2 + \tfrac{1}{24}r^4)\mu\delta^5 \pm r(\tfrac{1}{90} - \tfrac{1}{36}r^2 + \tfrac{1}{120}r^4)\delta^6 \\
&\quad - (\tfrac{1}{140} - \tfrac{7}{240}r^2 + \tfrac{1}{72}r^4 - \tfrac{1}{720}r^6)\mu\delta^7 \\
&\quad \mp r(\tfrac{1}{560} - \tfrac{7}{1440}r^2 + \tfrac{1}{480}r^4 - \tfrac{1}{5040}r^6)\delta^8 + \mathcal{O}(\delta^9)\,.
\end{aligned} \tag{6}$$

For microsimulators with Dirichlet boundary conditions, we adapt the earlier analysis of Roberts & Kevrekidis (2005). But instead of determining the slopes at the tooth boundaries as above, the following interpolation of

Table 1: Growth rates λ of perturbations from steady state $u = 0$: for diffusion (8) with m teeth, $H = 2\pi/m$; with gap to tooth ratio $r = 0.1$; $n = 11$ points in the microscale grid; and with the fourth order TBC (9).

m	1	2,3	4,5	6,7	$m+1:2m$
4	$6 \cdot 10^{-12}$	-0.946256	-2.166285	n/a	-397.2
8	$-3 \cdot 10^{-12}$	-0.996073	-3.785024	-7.121435	$-1588.$
16	$-1 \cdot 10^{-10}$	-0.999750	-3.984293	-8.832102	$-6355.$
32	0	-0.999986	-3.998999	-8.988613	$-25421.$

the macroscopic field determines the field values u on the edges of the teeth:

$$
\begin{aligned}
E^{\pm r} &= (1 + \mu\delta + \tfrac{1}{2}\delta^2)^{\pm r} \\
&= 1 \pm r\mu\delta + \tfrac{1}{2}r^2\delta^2 \pm \tfrac{1}{3!}r(r^2 - 1)\mu\delta^3 + \tfrac{1}{4!}r^2(r^2 - 1)\delta^4 \\
&\quad \pm \tfrac{1}{5!}r(r^2 - 1)(r^2 - 4)\mu\delta^5 + \tfrac{1}{6!}r^2(r^2 - 1)(r^2 - 4)\delta^6 \\
&\quad \pm \tfrac{1}{7!}r(r^2 - 1)(r^2 - 4)(r^2 - 9)\mu\delta^7 \\
&\quad + \tfrac{1}{8!}r^2(r^2 - 1)(r^2 - 4)(r^2 - 9)\delta^8 + \mathcal{O}(\delta^9).
\end{aligned}
\tag{7}
$$

The pattern in the above interpolation formula is clear. Now we explore the numerical performance of a gap-tooth scheme using this formula to determine teeth boundary conditions.

Consider gap-tooth simulations of the simple diffusion equation

$$
\frac{\partial u}{\partial t} = \frac{\partial^2 u}{\partial x^2}, \quad \text{and } 2\pi\text{-periodic in } x.
\tag{8}
$$

Imagine we only have access to the dynamics through a microscopic simulator of the diffusion (8), here coded by a fine discretisation on n grid points, spaced a distance $\eta = h/(n-1)$ apart, across a tooth of microscopic width $h = rH$. The time integration is an explicit scheme with a microscopic time step, typically $\Delta t = 10^{-6}$–10^{-4}. Figure 2 shows an example of the initially rapid microscopic evolution within one tooth; the microsimulator, coupled to its neighbors, rapidly evolves to a smooth state. Figure 3 similarly shows the initial evolution in two neighbouring teeth and how the smooth subgrid field arises through the coupling to the neighbouring teeth. Similar dynamics takes place during the initial instants of the Burgers' evolution shown in Figure 1.

Firstly we implement the following TBC. On the edge of the jth tooth, at $x = X_j \pm rH$, the boundary condition of the fine discretisation is that the field

$$
v_j = \left[1 \pm r\mu\delta + \tfrac{1}{2}r^2\delta^2 \pm \tfrac{1}{6}r(r^2 - 1)\mu\delta^3 + \tfrac{1}{24}r^2(r^2 - 1)\delta^4 \right] U_j.
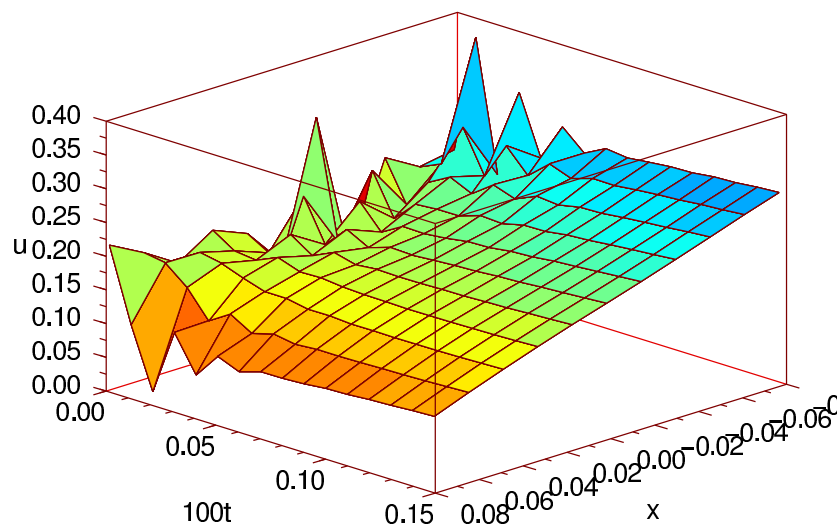\tag{9}
$$

Figure 2: view of the initial microscopic evolution within a tooth with dynamics described by the diffusion PDE (8) and coupled to its neighbours.
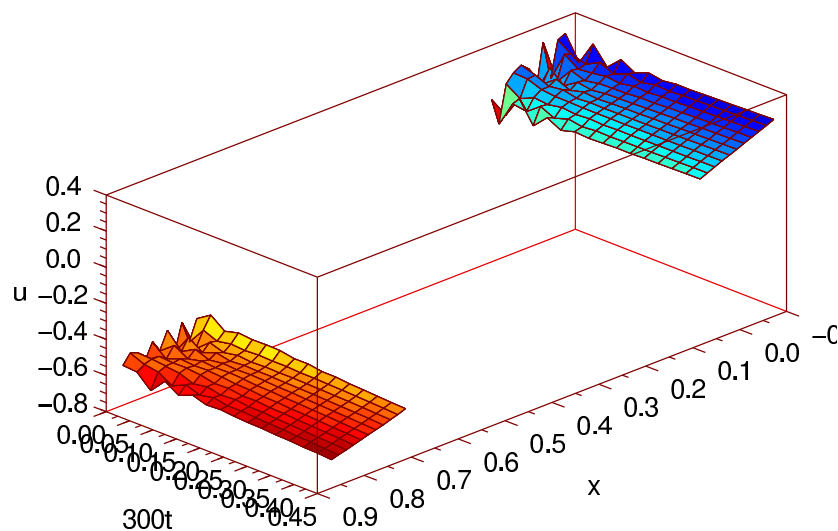

Figure 3: view of the initial microscopic evolution within a pair of neighbouring teeth with dynamics described by the diffusion PDE (8) and also coupled to their neighbours.

Table 2: Growth rates λ of perturbations from steady state $u = 0$: for diffusion (8) with m teeth, $H = 2\pi/m$; with gap to tooth ratio $r = 0.1$; $n = 11$ points in the microscale grid; and with the sixth order TBC.

m	1	2,3	4,5	6,7	$m + 1 : 2m$
4	$-5 \cdot 10^{-12}$	-0.981981	-2.453767	n/a	-397.2
8	$1 \cdot 10^{-11}$	-0.999653	-3.927925	-7.835158	$-1588.$
16	$8 \cdot 10^{-11}$	-1.000001	-3.998611	-8.966332	$-6355.$
32	$8 \cdot 10^{-10}$	-1.000002	-4.000004	-8.999518	$-25421.$

The first few terms of (7) provide this by interpolation from the surrounding coarse grid values. For the jth tooth this TBC involves macroscopic grid values $U_{j-2}, \ldots, U_{j+2}$ only, and thus we should be able to achieve $\mathcal{O}(H^4)$ consistency with the microsimulator. We numerically linearize the map over one microscopic time step by systematically perturbing each and every microscopic value from zero (there are mn such microscopic values, one for each of n fine grid points in each of m teeth). We then transform the eigenvalues μ of this map to growth rates $\lambda = \log(\mu)/\Delta t$. The mn growth rates fall into n groups of m modes. Each group corresponds to a microscopic *internal mode* of the dynamics; the mode is essentially the same in each tooth. Large negative growth rates correspond to rapidly decaying internal modes with significant microscopic structure within each tooth. The group of m modes with *small* growth rates correspond to the relatively slowly evolving *macroscopic* modes of interest that arise through the coupling of the microscopic dynamics across the teeth. Table 1 shows the leading seven growth rates, and the magnitude of the leading internal growth rate, for various numbers of teeth, $m = 4, 8, 16, 32$. The exact growth rates of the diffusion PDE (8) are $\lambda = -k^2$ for integer k. The table shows that as the number of teeth doubles, the accuracy of the growth rates of the macroscopic modes improves by a factor of about 16. This is consistent with an $\mathcal{O}(H^4)$ method as predicted for diffusion with TBC (9).

Table 2 shows the even higher order accuracy from implementing sixth order TBCs from (7)—growth rates slightly larger than the ideal seem to be due to the relatively small number of microscopic grid points within the teeth. These sixth order TBCs are used in the simulations of the nonlinear Burgers' equation shown in Figure 1. This simulation suggests that gap-tooth schemes employing such TBCs even for nonlinear systems are effective.

Table 3: Growth rates λ of perturbations from steady state $u = 0$: for diffusion (8) with m teeth, $H = 2\pi/m$; with gap to tooth ratio $r = 0.1$; $n = 11$ points in the microscale grid; and with the mixed TBC (10) with $a = 0.95$ and $b = 0.05$.

m	1	2,3	4,5	6,7	$m+1 : 2m$
4	$9 \cdot 10^{-12}$	-0.939448	-2.151772	n/a	-240.7
8	$-2 \cdot 10^{-11}$	-0.990854	-3.766007	-7.089004	-756.9
16	$7 \cdot 10^{-11}$	-0.996405	-3.971027	-8.803476	$-2417.$
32	$6 \cdot 10^{-10}$	-0.998047	-3.991243	-8.971213	$-8153.$

3   Mixed boundary conditions for the teeth

Let us explore mixed boundary conditions at the edges of the teeth: suppose the microsimulator requires $av_j \pm b\partial_x v_j$ specified on the edge of the teeth $x = x_j \pm rH$ for some constants a and b. The case $a = 1$ and $b = 0$ constitutes Dirichlet TBCs discussed in the previous section. The case $a = 0$ and $b = 1$ constitutes Neumann TBCs as discussed by Roberts & Kevrekidis (2005): there we used the interpolation formula (6) to specify slopes/fluxes on the edge of each tooth; we obtained spectra of accuracy similar to those in Tables 1 and 2.

For mixed TBCs we propose to simply combine (6) and (7) to give, for example, the fourth order in macroscopic grid size $H = 2\pi/m$ boundary condition

$$
\begin{aligned}
& av_j \pm b\partial_x v_j \\
& = a \left[1 \pm r\mu\delta + \tfrac{1}{2}r^2\delta^2 \pm \tfrac{1}{6}r(r^2 - 1)\mu\delta^3 + \tfrac{1}{24}r^2(r^2 - 1)\delta^4 \right] U_j \\
& \pm \frac{b}{H} \left[\mu\delta \pm r\delta^2 - (\tfrac{1}{6} - \tfrac{1}{2}r^2)\mu\delta^3 \mp r(\tfrac{1}{12} - \tfrac{1}{6}r^2)\delta^4 \right] U_j \\
& \text{on } x = x_j \pm rH.
\end{aligned}
\tag{10}
$$

We use $a = 0.95$ and $b = 0.05$ in the mixed TBC: this gives a mixed boundary condition where the effects of the function value v_j and its gradient $\partial_x v_j$ are roughly comparable in the TBC (if the parameter b is significantly larger, then the gradient term dominates the TBC). The numerical eigenvalues given in Table 3 for the diffusion equation (8) with these TBCs again show convergence to the correct eigenvalues as the number of teeth increases, that is, as the macroscopic grid size $H \to 0$. However, the convergence is not as rapid as for Dirichlet TBCs. The poorer convergence as $H \to 0$ seems to be due to the microscopic grid resolution: successive doubling of the number of interior points, see Table 4, demonstrates that there are significant errors of $\mathcal{O}(\eta^2)$

Table 4: Growth rates λ of perturbations from steady state $u = 0$: for diffusion (8) with $m = 8$ teeth; with gap to tooth ratio $r = 0.1$; n points in the microscale grid to show variation with microscale resolution; and with the mixed TBC (10) with $a = 0.95$ and $b = 0.05$.

n	1	2,3	4,5	6,7
11	$-2 \cdot 10^{-11}$	-0.990854	-3.766007	-7.089004
21	$1 \cdot 10^{-10}$	-0.994896	-3.781289	-7.117588
41	$-3 \cdot 10^{-10}$	-0.995792	-3.784677	-7.123924

in the microscale grid size η. Thus the total error in this implementation of the mixed TBCs seems to be $\mathcal{O}(H^4, \eta^2)$.

Here the microscale simulation is that of a fine discretisation of a PDE. Thus the derivatives in the mixed TBC (10) are subject to the significant errors of numerical differentiation when computed on the microscale. As Table 4 shows, the approximation of derivatives does incur errors; we would be better off without such errors. Higher order formulae for microscale interpolation would reduce the microscale errors in the boundary derivatives, perhaps from $\mathcal{O}(\eta^2)$ to $\mathcal{O}(\eta^4)$, but would ruin the small bandwidth of the microscale simulator. In any case, recall that we adopt the policy that we cannot change the microscale simulator as it is a legacy code handed to us from past development. We cannot (do not want to) change the nature nor accuracy of its boundary conditions. Consequently we proceed to address the problem of supplying boundary conditions at the edge of the teeth, *precisely as required during execution* of the legacy microscale simulator.

4   Teeth with two point boundary conditions

A microscale simulator may have implemented boundary conditions that do not fit into the classic partial differential equation form of Dirichlet, Neumann nor mixed. Here the microscale simulator implements a discretisation of 3 point stencil width. Consequently the simulator has been written so that the supplied boundary conditions only depend upon each of the two extreme pairs of points in each tooth. We thus investigate teeth boundary conditions that specify a combination of these two point values of the field at the edge of each tooth. This specific case is just one example of the wide range of possible nonlocal TBCs that specific microsimulators may require.

Suppose the microsimulator, here a fine spatial discretisation of the diffusion PDE (8), implements a tooth boundary condition of the (linear) form

Table 5: Growth rates λ of perturbations from steady state $u = 0$: for diffusion (8) with $m = 8$ teeth; with gap to tooth ratio $r = 0.1$; n points in the microscale grid to show variation with microscale resolution $\eta \propto 1/n$; and with the fourth order general TBC (12) with $\beta = 1$.

n	1	2,3	4,5	6,7
11	$1 \cdot 10^{-10}$	-0.999741	-3.984137	-8.831209
21	$-3 \cdot 10^{-10}$	-0.999742	-3.984159	-8.831368
41	$1 \cdot 10^{-9}$	-0.999742	-3.984169	-8.831453

$$v_{j,1} + \beta v_{j,2} \quad \text{and} \quad \beta v_{j,n-1} + v_{j,n} \quad \text{are specified}, \tag{11}$$

where $v_{j,i}$ denotes the microscale field value at the ith microscale grid point in the jth tooth. For example, the case $\beta = 1$ approximates Dirichlet boundary conditions at the microscale grid mid-points $x_{j,3/2}$ and $x_{j,n-1/2}$ near the edges of each tooth, which is exactly the case $a = 0$ and $b = 1$ implemented in the previous Section 3. Different values of β would *approximate* different mixed boundary conditions of the previous section.

The procedure is straightforward: we interpolate the macroscale grid values to find the specific values required by the boundary conditions (11). Recall that (9) gives a fourth order interpolation from the macroscale grid to points at the tooth boundaries $x = X_j \pm rH$; this gives appropriate values for $v_{j,1}$ and $v_{j,n}$. Get appropriate values for $v_{j,2}$ and $v_{j,n-1}$ through simply replacing in the formula the ratio $r = h/(2H)$ by the ratio required to reach the penultimate microgrid point, namely $r' = (h/2 - \eta)/H$, where $\eta = h/(n-1)$ is the microgrid size. Thus the fourth order version of the boundary condition (11) is that at $x = X_j \pm rH$

$$
\begin{aligned}
&(1 + \beta E^{\mp \eta/H})v_j \\
&= \left[1 \pm r\mu\delta + \tfrac{1}{2}r^2\delta^2 \pm \tfrac{1}{6}r(r^2-1)\mu\delta^3 + \tfrac{1}{24}r^2(r^2-1)\delta^4 \right] U_j \\
&+ \beta \left[1 \pm r'\mu\delta + \tfrac{1}{2}r'^2\delta^2 \pm \tfrac{1}{6}r'(r'^2-1)\mu\delta^3 + \tfrac{1}{24}r'^2(r'^2-1)\delta^4 \right] U_j.
\end{aligned}
\tag{12}
$$

Implementing the TBC (12) for the diffusion equation (8) gives a numerical approximation scheme with eigenvalues shown in Table 5 for varying microgrid resolution. See that there is only an extremely weak dependence upon the microgrid size η. *Thus implementing directly the boundary conditions that the microscale simulator actually expects during execution results in much better accuracy than trying to approximate the microscale TBCs using computed spatial derivatives.*

Table 6: Growth rates λ of perturbations from steady state $u = 0$: for diffusion (8) with m teeth, $H = 2\pi/m$; with gap to tooth ratio $r = 0.1$; $n = 11$ points in the microscale grid; and with the fourth order general TBC (12) with $\beta = 1$.

m	1	2,3	4,5	6,7	$m+1:2m$
4	$-8 \cdot 10^{-12}$	-0.946069	-2.165068	n/a	-489.5
8	$4 \cdot 10^{-11}$	-0.996034	-3.784277	-7.118312	$-1958.$
16	$1 \cdot 10^{-10}$	-0.999741	-3.984137	-8.831209	$-7832.$
32	$8 \cdot 10^{-10}$	-0.999983	-3.998964	-8.988427	$-31329.$

Lastly, Table 6 shows the eigenvalues of the gap-tooth scheme for varying number m of teeth in the domain. See that the eigenvalues converge to their correct values like $\mathcal{O}(H^4)$ as expected by the construction.

Higher order TBCs, in the macroscopic grid size H, would similarly be based upon the expansion (7). We then expect even more rapid convergence as the macroscale grid size $H \to 0$.

5   The model is independent of the tooth boundary conditions

Here we use analytic methods of holistic discretisation (Roberts 2001*b*, e.g.) to explore the gap-tooth scheme on a general class of PDEs with general mixed boundary conditions. The analysis establishes three important properties:

- the approach generates macroscopic models which are consistent with the microscopic dynamics to high orders in grid spacing H;

- the macroscopic model and the microscopic solution field are essentially independent of the size of the teeth, as parametrised by r; and

- the macroscopic model and the microscopic solution field are essentially independent of the details of the TBCs.

5.1   Theory underpins analysis of a PDE with tooth boundary conditions

We explore solutions of the class of *linear* hyper-advection-diffusion PDEs

$$\frac{\partial u}{\partial t} = \frac{\partial^2 u}{\partial x^2} - \epsilon \left(c\frac{\partial u}{\partial x} + b\frac{\partial^3 u}{\partial x^3} + a\frac{\partial^4 u}{\partial x^4} \right), \qquad (13)$$

where a, b and c are arbitrary parameters, and where ϵ is introduced as a convenient mechanism to control truncation in the multivariate power series solutions in the parameters a, b and c. This PDE is solved with mixed tooth boundary conditions inspired by (10), namely that on $x = x_j \pm rH$, and in terms of an artificial parameter γ that we explain shortly,

$$
\begin{aligned}
&\pm \alpha v_j + \partial_x v_j \\
&= \pm \alpha \left\{ 1 + \gamma r \left[\pm \mu \delta + \tfrac{1}{2} r \delta^2 \right] + \gamma^2 \tfrac{1}{6} r (r^2 - 1) \left[\pm \mu \delta^3 + \tfrac{1}{4} r \delta^4 \right] \right. \\
&\qquad \left. + \gamma^3 \tfrac{1}{120} r (r^2 - 1)(r^2 - 4) \left[\pm \mu \delta^5 + \tfrac{1}{6} r \delta^6 \right] \right\} U_j \\
&\quad + \frac{1}{H} \left\{ \gamma \left[\mu \delta \pm r \delta^2 \right] + \gamma^2 \left[-(\tfrac{1}{6} - \tfrac{1}{2} r^2) \mu \delta^3 \mp r(\tfrac{1}{12} - \tfrac{1}{6} r^2) \delta^4 \right] \right. \\
&\qquad \left. + \gamma^3 \left[(\tfrac{1}{30} - \tfrac{1}{8} r^2 + \tfrac{1}{24} r^4) \mu \delta^5 \pm r(\tfrac{1}{90} - \tfrac{1}{36} r^2 + \tfrac{1}{120} r^4) \delta^6 \right] \right\} U_j \\
&\quad + \mathcal{O}(\gamma^4).
\end{aligned}
\tag{14}
$$

Explore the structure of this complicated looking TBC: $\pm \alpha v_j + \partial_x v_j$ represents a general linear combination of the microscopic field at the edge of each tooth that needs to be specified for the microscopic simulator; those terms in the right-hand side multiplied by $\pm \alpha$ form the estimate of the field v_j interpolated from the surrounding macroscopic grid values; those terms in the right-hand side multiplied by $1/H$ form the estimate of the field's gradient $\partial_x v_j$ interpolated from the surrounding macroscopic grid values. However, these two interpolations only hold when the artificial parameter $\gamma = 1$; one is the physically interesting value of γ. Why then do we introduce the parameter γ? The reason is that, as in "discretisation" (Roberts 2001a), based around the special values of the parameters $\gamma = \alpha = \epsilon = 0$, the general PDE (13) with TBC (14) possesses a (slow) centre manifold parametrised by the macroscopic grid values. On this centre manifold the evolution of these macroscopic grid values forms a macroscale model of the PDE. This model has rigorous theoretical support based upon $\gamma = 0$, and it becomes physically relevant when evaluated at $\gamma = 1$.

We briefly explain how centre manifold theory underpins the macroscale model. Initially set $\gamma = \alpha = \epsilon = 0$; then the PDE+TBC become the diffusion equation with *insulating* boundaries at the edges of the teeth, $x = x_j \pm rH$. Thus, exponentially quickly, all structure within each tooth diffuses away to become constant, but a different constant for each tooth depending upon the initial conditions. See a similar evolution in Figures 2 and 3; but there the teeth are coupled, so that the rapid evolution is to a smooth variation in each tooth, whereas here the insulated evolution, $\gamma = \alpha = \epsilon = 0$, is to a constant in each tooth. But we are only interested in fully coupled teeth for which $\gamma = 1$, and in non-zero α and ϵ. Thus from the simple base of

piecewise constant fields, we construct a description of the field u and its slow evolution as a power series in the "perturbations" measured by γ, α and ϵ. The departure of the field u from a constant within each tooth gives the microscopic (subgrid, subtooth) field, as shown for example in the smooth fields of Figures 2 and 3 that are quickly established. The slow evolution of the coarse grid values U_j gives the macroscopic model.

The various powers of γ in the TBC (14) are chosen so that truncation of the expressions to errors $\mathcal{O}(\gamma^p)$ will generate a discrete macroscopic model expressing $\dot{U}_j$ in terms of only $U_{j-p+1}, \ldots, U_{j+p-1}$ (a spatial stencil of width $2p - 1$). Centre manifold theory (Carr 1981, Kuznetsov 1995, e.g.) asserts that

- such a model exists,

- that through its exponential attractiveness, the model is relevant in some finite neighbourhood of $\gamma = \alpha = \epsilon = 0$,

- and that we may systematically construct the power series approximation to the model.

Because truncation to errors $\mathcal{O}(\gamma^p)$ results in a model with stencil width $2p-1$, *such a truncation corresponds to the gap-tooth scheme utilising* TBC*s involving interpolation from only the* $2p-1$ *neighbouring grid values* $U_{j-p+1}, \ldots, U_{j+p-1}$.

Computer algebra[1] performs all the tedious details of constructing the model (Roberts 1997). We seek a model where the subtooth/subgrid field

$$u(x, t) = v_j(x, \mathbf{U}; \alpha, \gamma, \epsilon) . \tag{15}$$

That is, the subtooth field has some spatial structure, such as that in Figures 2 and 3, which: depends upon the neighbouring grid values $U_{j-p+1}, \ldots, U_{j+p-1}$; may depend upon the specific TBC through its parameter α; depends upon the specific PDE though its parameter ϵ; and depends upon the coupling parameter γ. Centre manifold theory assures us the evolution of the system is governed by the evolution of the grid values:

$$\dot{U}_j = g_j(\mathbf{U}; \alpha, \gamma, \epsilon) ; \tag{16}$$

this formula is the macroscopic (closed) discretisation. We solve by iteration the PDE (13) with TBC (14) to find the centre manifold (15) and its associated coarse discretisation (16). The results are expressions for the microscopic fields v_j and the macroscopic evolution, $\dot{U}_j = g_j$, that are accurate to some specified order in the small parameters α, γ and ϵ.

---

[1]`http://www.sci.usq.edu.au/staff/aroberts/CA/burgermixed.red` is the source script which was available at the time of writing.

5.2 Modelling $\mathcal{O}(\epsilon)$ changes to the PDE

The subgrid fields in each tooth will in general depend upon the coefficients a, b and c that determine the PDE. For example, there are nontrivial dependencies upon the advection speed that ensure the macroscale model naturally transforms to an upwind discretisation for large advection speeds c (Roberts 2002)—such influences show up in the $\mathcal{O}(\epsilon^2)$ terms that we explore in the next subsection. Here we first explore the models linear in a, b and c, that is, linear in the general changes to the PDE (13) with the TBC (14).

For example, to errors $\mathcal{O}(\alpha^3, \gamma^4, \epsilon^2)$, computer algebra generates the macroscopic evolution

$$
\begin{aligned}
\dot{U}_j \;=\; & \frac{1}{H^2}\left[\gamma\delta^2 - \tfrac{1}{12}\gamma^2\delta^4 + \tfrac{1}{90}\gamma^3\delta^6\right]U_j \\
& - \frac{\epsilon c}{H}\left[\gamma\mu\delta - \tfrac{1}{6}\gamma^2\mu\delta^3 + \tfrac{1}{30}\gamma^3\mu\delta^5\right]U_j \\
& - \frac{\epsilon b}{H^3}\left[\gamma^2\mu\delta^3 - \tfrac{1}{4}\gamma^3\mu\delta^5\right]U_j \\
& - \frac{\epsilon a}{H^4}\left[\gamma^2\delta^4 - \tfrac{1}{6}\gamma^3\delta^6\right]U_j + \mathcal{O}(\alpha^3, \gamma^4, \epsilon^2).
\end{aligned}
\tag{17}
$$

When evaluated at the physically relevant parameter $\gamma = 1$ these are the classical finite difference operators for the PDE (13), truncated to $\mathcal{O}(\delta^7)$. Consequently the terms in the macroscopic model (17) are *consistent* with the PDE (13) to various orders in the macroscopic grid size H. The order of consistency depends upon the order of truncation in the artificial coupling parameter γ and the order of the derivatives in each term. *Observe that the macroscopic evolution operator is* independent *of r, the size of the teeth, and* independent *of α which parametrises the precise nature of the TBC (14).*

Now we explore the microscopic field within the teeth. To low order in the coupling parameter γ and in terms of the microscopic tooth space variable $\xi = (x - X_j)/H$, we find

$$
\begin{aligned}
v_j \;=\; & U_j + \gamma\left\{\left[\xi\mu\delta + \tfrac{1}{2}\xi^2\delta^2\right]\right. \\
& + \epsilon cH\left[(\tfrac{1}{6}\xi^3 - \tfrac{1}{2}r^2\xi) + \tfrac{1}{3}H\alpha r^3\xi - \tfrac{1}{3}H^2\alpha^2 r^4\xi\right]\delta^2\left.\right\}U_j \\
& + \mathcal{O}(\alpha^3, \gamma^2, \epsilon^2).
\end{aligned}
\tag{18}
$$

The first line gives the classic quadratic interpolation through the grid values U_j and $U_{j\pm1}$. The second line shows microscopic field structure in the advection speed c. But it exhibits undesirable dependence upon the tooth width r and nature α of the TBC. However, inspect the next order terms in coupling parameter γ:

$$
v_j \;=\; \cdots + \gamma^2\left\{\left[\tfrac{1}{6}(-\xi + \xi^3)\mu\delta^3 + \tfrac{1}{24}(-\xi^2 + \xi^4)\delta^4\right]\right.
$$

$$+ \epsilon c H \left[-(\tfrac{1}{6}\xi^3 - \tfrac{1}{2}r^2\xi) - \tfrac{1}{3}H\alpha r^3\xi + \tfrac{1}{3}H^2\alpha^2 r^4\xi \right] \delta^2$$
$$+ (-\tfrac{1}{18}\xi^3 + \tfrac{1}{60}\xi^5 + \tfrac{1}{6}r^2\xi - \tfrac{1}{12}r^2\xi^3 \tfrac{1}{6}r^4\xi)\delta^4$$
$$+ \alpha H(-\tfrac{1}{9}r^3\xi + \tfrac{1}{18}r^3\xi^3 - \tfrac{4}{15}r^5\xi)\delta^4$$
$$+ \alpha^2 H^2(\tfrac{1}{9}r^4\xi - \tfrac{1}{18}r^4\xi^3 + \tfrac{17}{45}r^6\xi)\delta^4$$
$$+ \frac{\epsilon b}{H} \left[-(\tfrac{1}{6}\xi^3 - \tfrac{1}{2}r^2\xi) - \tfrac{1}{3}H\alpha r^3\xi + \tfrac{1}{3}H^2\alpha^2 r^4\xi \right] \delta^4 \Big\} U_j$$
$$+ \mathcal{O}(\alpha^3, \gamma^3, \epsilon^2)\,; \tag{19}$$

The dots denote the terms given in the right-hand side of (18). The first line in the above higher order terms contains reassuringly the classic quartic interpolation formulae. The second line, when we set $\gamma = 1$, cancels all the undesirable α and r dependence in the lower order (18). The third and later lines above describe higher order microscopic structure; some of this undesirably depends upon the TBC through α and the size of the teeth through r, but as far as we have explored, any α and r dependence introduced at any order in γ is canceled by terms at higher orders in γ. Thus any finite truncation of the power series expansion for the model may have undesirable dependence upon α and r, but as the order in the artificial parameter γ is increased, this dependence is removed. In this sense, the microscopic field is "essentially" independent of the details of the TBC and independent of the tooth width r.

5.3   Modelling $\mathcal{O}(\epsilon^2)$ effects in the PDE

In our analysis we find that even order operators in the microscale PDE, such as the diffusion u_{xx} and the hyper-diffusion au_{xxxx}, are represented simply in the macroscale discretisation. However, odd order operators in the microscale PDE, such as advection cu_x and the dispersion bu_{xxx}, create nontrivial effects; these first show up in terms quadratic in their amplitude and hence they first appear in terms of $\mathcal{O}(\epsilon^2)$. We now show that the effects of $\mathcal{O}(\epsilon^2)$ terms typically act to stabilise the $\mathcal{O}(\epsilon)$ discrete model. The implication for the gap-tooth method is that the resolution of the subgrid structures by the microscale simulator will also typically maintain stability of the discrete macroscale model. That is, the microscale simulator will provide successful closure for the macroscale discretisation when coupled with the proposed TBCs.

To illustrate this, we can construct the approximate model of the PDE (13) with TBC (14) to errors $\mathcal{O}(\alpha^2, \gamma^4, \epsilon^3)$; that is, we include quadratic effects in the coefficients a, b and c. The details of the model are too long to record here. However, we find that the equivalent PDE to the macroscale discrete

model (17) with its $\mathcal{O}(\epsilon^2)$ modifications is

$$
\begin{aligned}
\frac{\partial u}{\partial t} = {} & \gamma\frac{\partial^2 u}{\partial x^2} - \epsilon\left[\gamma c\frac{\partial u}{\partial x} + \gamma^2 b\frac{\partial^3 u}{\partial x^3} + \gamma^2 a\frac{\partial^4 u}{\partial x^4}\right] \\
& + \epsilon^2\left[-(\gamma-\gamma^2)bc\frac{\partial^2 u}{\partial x^2} - (\gamma^2-\gamma^3)b^2\frac{\partial^4 u}{\partial x^4}\right] \\
& + H^2\left\{\tfrac{1}{12}(\gamma-\gamma^2)\frac{\partial^4 u}{\partial x^4}\right. \\
& \quad + \epsilon\left[-\tfrac{1}{6}(\gamma-\gamma^2)c\frac{\partial^3 u}{\partial x^3} - \tfrac{1}{4}(\gamma^2-\gamma^3)b\frac{\partial^5 u}{\partial x^5} - \tfrac{1}{6}(\gamma^2-\gamma^3)a\frac{\partial^6 u}{\partial x^6}\right] \\
& \quad + \epsilon^2\left[+\tfrac{1}{3}(\gamma-\gamma^2)c^2 r^2\frac{\partial^2 u}{\partial x^2} - \tfrac{1}{12}(\gamma-5\gamma^2+4\gamma^3)bc\frac{\partial^4 u}{\partial x^4}\right. \\
& \quad\quad \left.\left. + \tfrac{2}{3}(\gamma^2-\gamma^3)bcr^2\frac{\partial^4 u}{\partial x^4} - \tfrac{1}{6}(\gamma^2-7\gamma^3+4\gamma^3 r^2)b^2\frac{\partial^6 u}{\partial x^6}\right]\right\} \\
& + \mathcal{O}(H^3,\alpha^2,\gamma^4,\epsilon^3)\,.
\end{aligned}
\tag{20}
$$

Observe that to this level of accuracy there is no dependence upon the TBC parameter α, thus our comments apply for all the TBCs. Now consider the components of (20) in turn. The first line of (20) is the original general linear PDE (13) when evaluated at the physically meaningful $\gamma = 1$. The second line shows some error terms, quadratic in ϵ, that disappear for $\gamma = 1$. The bcu_{xx} error disappears when $\mathcal{O}(\gamma^2)$ terms are retained, which is as soon as the discretisation stencil is wide enough to model the third order dispersion term bu_{xxx}. The $b^2 u_{xxxx}$ dispersion-induced term shows that the method initially incorporates its effects as enhanced dissipation, as the coefficient of γ^2 is negative; then, when higher order accuracy is requested by retaining $\mathcal{O}(\gamma^3)$ terms, the method proceeds to remove the incurred error via the γ^3 term.

Consider applying these TBC to a microscale simulator; for slow enough spatial variations, the microsimulator is equivalent to some 'infinite order' PDE. For example, the *microscale* discretisation $\dot{u}_i = (1/\eta^2)\delta^2 u_i$ is, by (4), equivalent to the PDE $u_t = (4/\eta^2)\sinh^2(\eta\partial_x/2)u$. We expect the behaviour of errors in the gap-tooth scheme seen here, induced by the u_{xxx} and u_{xxxx} terms, be representative of the behaviour of errors in the 'high order' equivalent terms of any given microscopic simulator.

The remaining terms in (20) are $\mathcal{O}(H^2)$ and hence vanish as the macroscopic grid size $H \to 0$. Nonetheless look at the H^2 terms in the third to sixth lines as they apply to simulations with finite H. The third and fourth lines show that the initial discretisation errors of the linear terms are eliminated, for the physical $\gamma = 1$, via the next higher order in coupling parameter γ.

The particular focus of this subsection is the ϵ^2 terms on the next two lines. The $c^2 u_{xx}$ terms show that at low order truncations in γ the method treats advection in a manner that increases dissipation, as the coefficient is positive, and thus helps to maintain the stability of the macroscale discretisation to high advection speeds c (explored in Roberts 2001a, 2002). The interaction between advection cu_x and dispersion bu_{xxx} can maintain stability or be destabilising depending upon the sign of bc: whether we truncate at γ when $-bcu_{xx}$ dominates (second line) or we truncate at γ^2 when bcu_{xxxx} dominates (fifth and sixth lines), the combination is stabilising whenever $bc < 0$, that is, when the phase velocity of wave-like effects does not change direction as a function of wavenumber. The last term on the sixth line will be dominated by the dissipative $b^2 u_{xxxx}$ term on the second line, and we presume will vanish at higher orders in the coupling parameter γ. Thus, from the equivalent PDE (20) of the macroscale model, we deduce that the subgrid scale interactions between processes in the PDE, and hence for microscale simulators in general, are accounted for in this approach to generate a macroscale model that is typically stable.

Indeed this equivalent PDE (20) confirms support for the gap-tooth scheme with TBC by centre manifold theory. Theory asserts that the original system, here the PDE (20), and the centre manifold model, here the macroscale discretisation (16), have the same stability. Thus when the microscale system is stable, so will the macroscale discretization. The caveat is that we can only construct the centre manifold approximately; we control the errors to some order in the parameters α γ and ϵ, but there will be some error, albeit of high order in the parameters.

6 Conclusion

We use macroscale interpolation based upon the expansions (6) and (7) to determine TBCs for the boundary conditions at the edge of the teeth in the gap-tooth scheme. The interpolation was used to implement *directly* whatever boundary conditions are *actually* needed by the microscale legacy code during execution. Figure 4 shows a simulation of the nonlinear Burgers' equation with 2 point boundary conditions at the boundaries of each tooth as an illustrative example. We found that the macroscopic models resulting from the microsimulator and the constructed TBC were consistent, to high order, with the microscopic dynamics; that the macroscopic models and the microscopic (subgrid, subtooth) fields were essentially independent of the tooth size and the detailed nature of the TBC. We expect the same type of TBC to be effective for microsimulations in more than one spatial dimension.
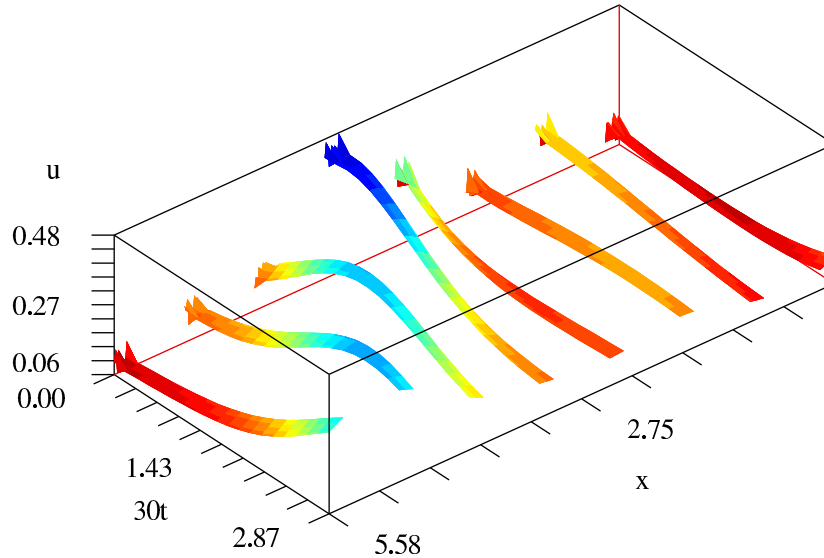
Tony Roberts, June 12, 2006

Figure 4: simulation of Burgers' equation using general 2-point boundary condition on the teeth of the fourth order (12) with $\beta = 1$ demonstrates the method is stable even for nonlinear PDEs.

Interesting future research would seek TBC that do not require communication across the gaps between the teeth at each and every microscale time step, and the interplay of TBCwith implicit integration schemes.

Further exciting research would explore issues of existence and performance of TBCs for stochastic microsimulators.

References

Balakotaiah, V. & Chang, H.-C. (2003), 'Hyperbolic homogenized models for thermal and solutal dispersion', *SIAM J. Appl. Math.* **63**, 1231–1258. http://epubs.siam.org/sam-bin/dbq/article/36886.

Carr, J. (1981), *Applications of centre manifold theory*, Vol. 35 of *Applied Math. Sci.*, Springer–Verlag.

Chen, Z. & Hou, T. Y. (2002), 'A mixed multiscale finite element method for elliptic problems with oscillating coefficients', *Math. Comp.* **72**, 541–576.

Chorin, A. J. & Stinis, P. (2005), Problem reduction, renormalization, and memory, Technical report, [`http://arXiv.org/abs/math.NA/0503612`].

Dolbow, J., Khaleel, M. A. & Mitchell, J. (2004), Multiscale mathematics initiative: A roadmap. report from the 3rd DoE workshop on multiscale mathematics, Technical report, Department of Energy, USA, `http://www.sc.doe.gov/ascr/mics/amr`.

Ei, S.-I., Fujii, K. & Kunihiro, T. (2000), 'Renormalization-group method for reduction of evolution equations: invariant manifolds and envelopes', *Annals of Physics* **280**, 236–298.

Gear, C. W., Li, J. & Kevrekidis, I. G. (2003), 'The gap-tooth method in particle simulations', *Phys. Lett. A* **316**, 190–195.

Gustafsson, B. & Mossino, J. (2003), 'Non-periodic explicit homogenization and reduction of dimension: the linear case', *IMA Journal of Applied Mathematics* **68**, 269–298. `http://dx.doi.org/10.1093/imamat/68.3.269`.

Hou, T. Y. & Wu, X.-H. (1997), 'A multiscale finite element method for elliptic problems in composite materials and porous media', *J. Comput. Phys* **134**, 169–189.

Kevrekidis, I. G., Gear, C. W., Hyman, J. M., Kevrekidis, P. G., Runborg, O. & Theodoropoulos, K. (2003), 'Equation-free, coarse-grained multiscale computation: enabling microscopic simulators to perform system level tasks', *Comm. Math. Sciences* **1**, 715–762.

Kuznetsov, Y. A. (1995), *Elements of applied bifurcation theory*, Vol. 112 of *Applied Mathematical Sciences*, Springer–Verlag.

Mudavanhu, B. & O'Malley, R. E. (2003), A new renormalization method for the asymptotic solution of weakly nonlinear vector systems, University of Washington.

National Physical Laboratory (1961), *Modern Computing Methods*, Vol. 16 of *Notes on Applied Science*, Her Majesty's Stationary Office.

Roberts, A. J. (1997), 'Low-dimensional modelling of dynamics via computer algebra', *Computer Phys. Comm.* **100**, 215–230.

Roberts, A. J. (2001*a*), 'Holistic discretisation ensures fidelity to Burgers' equation', *Applied Numerical Modelling* **37**, 371–396.

Roberts, A. J. (2001*b*), Holistic discretisation illuminates and enhances the numerical modelling of differential equations, *in* V. V. Kluev & N. E. Mastorakis, eds, 'Topics in Applied and Theoretical Mathematics and Computer Science', WSES Press, pp. 81–89.

Roberts, A. J. (2002), 'A holistic finite difference approach models linear dynamics consistently', *Mathematics of Computation* **72**, 247–262. `http://www.ams.org/mcom/2003-72-241/S0025-5718-02-01448-5`.

Roberts, A. J. & Kevrekidis, I. G. (2005), Higher order accuracy in the gap-tooth scheme for large-scale dynamics using microscopic simulators, *in* R. May & A. J. Roberts, eds, 'Proc. of 12th Computational Techniques and Applications Conference CTAC-2004', Vol. 46 of *ANZIAM J.*, pp. C637–C657. `http://anziamj.austms.org.au/V46/CTAC2004/Robe` [July 20, 2005].

Samaey, G., Kevrekidis, I. G. & Roose, D. (2004), Damping factors for the gap-tooth scheme, *in* S. Attinger & P. Koumoutsakos, eds, 'Multiscale Modeling and Simulation', Vol. 39 of *Lecture Notes in Computational Science and Engineering*, Springer–Verlag, pp. 93–102.

Samaey, G., Kevrekidis, I. G. & Roose, D. (2005), 'The gap-tooth scheme for homogenization problems', *SIAM Multiscale Modeling and Simulation* **4**, 278–306. `http://epubs.siam.org/sam-bin/dbq/article/60204`.